

# Combined State and Parameter Estimation of Lithium-Ion Battery with Active Current Injection

Ziyou Song<sup>a</sup>, Member, IEEE, Hao Wang<sup>a</sup>, Jun Hou<sup>b\*</sup>, Member, IEEE, Heath Hofmann<sup>b</sup>, Senior Member, IEEE,  
and Jing Sun<sup>a</sup>, Fellow, IEEE

<sup>a</sup> Department of Naval Architecture and Marine Engineering, University of Michigan, Ann Arbor, MI 48109, USA

<sup>b</sup> Department of Electrical Engineering and Computer Science, University of Michigan, Ann Arbor, MI 48109, USA

**Abstract**—Estimating the State of Charge (SoC) and State of Health (SoH), together with the parameters used in representing the dynamics of a Lithium-ion battery, is essential to ensure optimal and reliable operation. However, this simultaneous estimation can take a significant amount of time to converge, and the estimation accuracy is limited by measurement noise and model inaccuracy. Note that for over-actuated systems (e.g., hybrid energy storage systems and hybrid electric vehicles), the over-actuation feature can be exploited to optimize the battery current profile for the estimation purpose. This paper shows the potential to improve estimation accuracy when the desired current is actively injected and the estimation algorithm is properly structured. Specifically, by incorporating a high-pass filter, battery parameters can be independently characterized by injecting high-frequency and medium-frequency currents, and battery SoC/SoH can then be estimated sequentially from the estimated parameters. A Cramer-Rao bound analysis shows that the accuracy of the proposed sequential estimation is much better than the case where all parameters and states are simultaneously estimated. The analysis is verified by simulation and experimental results. We point out that for battery-only applications (e.g., electric vehicles), the proposed method has limitations as generally the battery current profile cannot be changed.

## I. INTRODUCTION

Lithium-ion batteries have been widely used in many applications, such as electric vehicles and renewable energy systems [1]. Online monitoring of State of Charge (SoC) and State of Health (SoH) plays an important role in ensuring safe, reliable, and efficient operation [2]. However, when simultaneously estimating all parameters and states of the battery, the estimation can take a significant amount of time to converge, and its accuracy can be compromised when considering model uncertainty and measurement noise [3].

Most of the literature on battery state and parameter estimation has focused on battery models [4] and estimation algorithms [5]. While these studies are important, the input-output data used plays a significant role in the estimation performance [6]. A persistently exciting (PE) input condition must be necessarily satisfied to ensure that all parameters can converge to the actual values [7]. In addition, most existing estimation approaches use the data indiscriminately without

exploiting the sensitivity of the data to the specific parameters to be identified [8]. The estimation accuracy will be impaired when data without a sufficient “richness” is used [9], [10].

In recent years more attention has been paid to the impact of data on estimation performance. Analytical results provided in [11] and [12] use the Fisher information matrix and Cramer-Rao (CR) bounds to analyze the influence of data on estimation accuracy. Rothenberger et al. optimized the battery current profile to maximize the Fisher information matrix for a better estimation performance [13], [14]. Lin et al. derived analytic bounds on the estimation accuracy of SoC, capacity, and ohmic resistance under various circumstances [6]. The connection between the excitation and the SoC estimation error considering measurement noise/bias [15], model uncertainties [16], and estimation algorithms have also been addressed.

However, in the case where all battery parameters and states are estimated simultaneously, the estimation performance is limited even when the battery current profile is well-designed [17]. This is caused by the fact that the state and parameter estimation problems are inherently intertwined, and noise is introduced in the measurement. The separation of state and parameter estimation, which could lead to reduced uncertainty in each estimation problem, however, has not been explored. Based on analysis of the first-order equivalent circuit model (ECM), it has been shown that it is possible to estimate battery parameters/states sequentially by incorporating a high-pass filter and actively injecting current signals to improve the estimation accuracy. Performance of the sequential algorithm has also been demonstrated [18]. Such a sequential algorithm is therefore adopted in this study. We note that the sequential algorithm was designed for over-actuated systems (e.g., hybrid electric vehicles and the battery/supercapacitor hybrid energy storage system), since the over-actuation feature can be exploited for the active current injection.

This paper focuses on establishing the properties of the sequential algorithm and the optimization of the inputs for estimation. The main contributions of this paper include the following aspects. First, the time-averaged CR bound, which indicates the lower bound of the estimation error

This material is based upon work supported by U.S. Office of Naval Research (ONR) under Grants N00014-16-1-3108 and N00014-18-2330. We also would like to thank Dr. Xiaogang Wu and Mr. Xuefeng Li from Harbin University of Science and Technology, China for their help with the experiments.

covariance of unbiased estimation, is used to establish the advantage of the sequential algorithm when compared to the multi-parameter case where all parameters and states are estimated concurrently. Second, the influence of frequency on the estimation performance is investigated for the sequential algorithm to optimize the current profile. Third, simulations are conducted considering noise, and the effectiveness of the sequential algorithm is validated. Finally, initial experimental results are provided to further verify the proposed algorithm.

The rest of the paper is organized as follows. In Section 2, the first-order ECM battery model is described and the dynamics are analyzed. In Section 3, the time-averaged CR bound is briefly introduced and the CR bound analysis is performed. Simulation results are shown in Section 4. Experimental results are presented in Section 5. Conclusions are given in Section 6.

## II. SYSTEM DESCRIPTION

The state estimation of Lithium-ion batteries, including battery SoC and SoH, is an important task in practical applications. To perform this task, model-based algorithms have been widely studied. Generally, the model parameters are significantly influenced by battery degradation and operating conditions, therefore the model parameters should be estimated together with the battery states. However, it is challenging to simultaneously estimate all parameters and states given model inaccuracy, uncertainties, and measurement noise. In this section the battery dynamics are analyzed, and the possibility of separating different dynamic components in the frequency domain is investigated to decompose the coupled estimation problem.

There are various models for lithium-ion batteries, such as the equivalent circuit model (ECM) [4], impedance model [19], and electrochemical model [20]. While the more complex models (e.g., the electrochemical model) are more accurate, the first-order ECM is widely used in practical applications given its simplicity and sufficient accuracy [4]. We point out that, even though the analysis in this paper focuses on the first-order ECM, the proposed methodology can be generalized to other models. As shown in Fig. 1, the battery terminal voltage and current are denoted as  $v_b$  and  $i_b$ , respectively. The ECM dynamics can be presented as follows:

$$\begin{cases} \dot{v}_c = -\frac{1}{C_t R_t} v_c + \frac{1}{C_t} i_b, \\ v_b = v_{oc} - R_s i_b - v_c, \end{cases} \quad (1)$$

where  $v_c$  is the voltage of RC pair. The OCV-SoC relationship is given as [21]

$$v_{oc}(z) = K_0 - \frac{K_1}{z} - K_2 z + K_3 \ln(z) + K_4 \ln(1-z), \quad (2)$$

where  $K_{0-4}$  are the model coefficients and  $z$  is the normalized SoC. The SoC dynamic is described as [22]

$$z = z_0 - \int_{t_0}^t \frac{\eta}{Q_b} i_b(t) dt, \quad (3)$$

where  $z_0$  is the initial SoC,  $\eta$  is the charging/discharging

efficiency,  $t_0$  is the start time, and  $Q_b$  is the battery capacity. The slope of the OCV-SoC curve is constant for most battery chemistries within the normal operating range [23], [24]. Consequently, Eq. (2) is linearized to simplify the CR bound analysis in the following section.

$$v_{oc}(t) = a \left( z_0 - \int_{t_0}^t \frac{\eta i_b(v)}{Q_b} dv \right) + b, \quad (4)$$

where  $a$  and  $b$  are the coefficients of the linearized OCV-SoC function. The battery SoC and SoH are represented by  $z_0$  and  $Q_b$ , respectively. An 18650 Lithium-ion battery cell made by Samsung® is considered, and its parameters are listed in Table 1. The coefficients  $K_{0-4}$  of the OCV-SoC for the adopted cell are 2.6031, 0.0674, -1.527, 0.6265, and -0.0297, respectively. The battery parameters and OCV-SoC coefficients were obtained by conducting Hybrid Pulse Power Capability (HPPC) and Static Capacity tests on the adopted battery cell.

For the combined state and parameter estimation problem studied in this paper, the following assumptions can be made:

1) The initial value of  $v_c$  is 0,

2) The values of  $R_s$ ,  $R_t$ , and  $\tau$  are constant in the estimation process, since they vary much more slowly than the battery SoC [25].

Based on Eqs. (1)-(3), the transfer function from  $i_b$  to  $v_b$  can be given as

$$v_b(s) = \left[ \frac{az_0 + b}{s} \right] - \left[ \frac{a}{s} \frac{\eta}{Q_b} i_b(s) \right] - \left[ R_s i_b(s) \right] - \left[ \frac{R_t}{1 + \tau s} i_b(s) \right], \quad (5)$$

where  $s$  is the complex Laplace variable. Note that the battery terminal voltage expression includes four components, with each term associated with a specific subset of parameters. The first term is due to the initial SoC. The second is related to the SoC variation, and is significantly influenced by the battery capacity  $Q_b$ . The third and fourth components are related to the ohmic resistance and the RC pair, respectively.

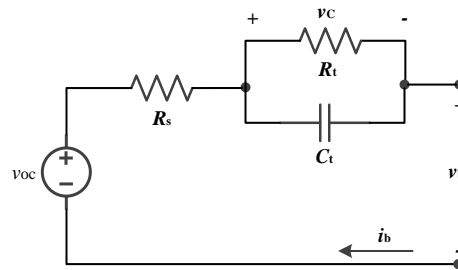


Fig. 1. First-order equivalent circuit model for battery.

TABLE I

Specification for the 18650 battery cell

Parameter	Value
Nominal Voltage (V)	3.63
Cell Capacity (Ah)	2.44
Ohmic Resistance $R_s$ ( $\mu\Omega$ )	~100
Diffusion Resistance $R_t$ ( $\mu\Omega$ )	~30
Time Constant $\tau$ (s)	~15
Discharge/Charge Efficiency $\eta$ (%)	98
OCV-SoC Slope $a$ (mV/100%)	~8.845
Voltage Measurement Noise $\sigma_v$ (mV)	20

These four components of the battery voltage have significantly different characteristics in the frequency domain, a property will be exploited in this paper by incorporating filters and actively injecting current signals that decompose the state and parameter estimation problem.

Consider passing the battery voltage and current measurements through a first-order high-pass filter:

$$v_{bf}(s) = \frac{T_c s}{1 + T_c s} v_b(s), \quad i_{bf}(s) = \frac{T_c s}{1 + T_c s} i_b(s),$$

where  $T_c$  is the time coefficient of the high-pass filter, and  $v_{bf}$  and  $i_{bf}$  are the filtered battery voltage and current, respectively. The filtered system can be described as

$$v_{bf}(s) = v_{c1}(s) - v_{c2}(s) - v_{c3}(s) - v_{c4}(s) \quad (6)$$

$$\text{where } v_{c1}(s) = \frac{(az_0 + b)T_c}{1 + T_c s}, \quad v_{c2}(s) = \frac{a}{s} \frac{\eta}{Q_b} i_{bf}(s),$$

$$v_{c3}(s) = R_s i_{bf}(s), \quad v_{c4}(s) = \frac{R_t}{1 + \tau_s} i_{bf}(s),$$

and  $v_{c1}$ ,  $v_{c2}$ ,  $v_{c3}$ , and  $v_{c4}$  are the terms associated with filtered initial SoC, SoC variation, ohmic resistance, and RC pair voltage components, respectively. After filtering, the response to the initial SoC is given as

$$v_{c1}(t) = \mathcal{L}^{-1} \left\{ \frac{(az_0 + b)T_c}{1 + T_c s} \right\} = (az_0 + b)e^{-\frac{t}{T_c}} \rightarrow 0 \quad (7)$$

which will vanish over time and can therefore be neglected. A sinusoidal battery current, which is frequently used for parameter estimation, is considered to analyze the battery dynamics:

$$\begin{cases} i_b(t) = M \cos(\omega t), \\ i_b(s) = \frac{Ms}{s^2 + \omega^2}, \end{cases} \quad (8)$$

where  $M$  is the current magnitude and  $\omega$  is the current frequency. The filtered voltage components  $v_{c2}$ ,  $v_{c3}$ , and  $v_{c4}$  asymptotically converge to

$$\begin{cases} v_{c2}(t) \rightarrow -M a \eta T_c \frac{T_c \omega \sin(\omega t) - \cos(\omega t)}{Q_b (1 + T_c^2 \omega^2)}, \\ v_{c3}(t) \rightarrow -M R_s T_c \omega \frac{T_c \omega \cos(\omega t) - \sin(\omega t)}{1 + T_c^2 \omega^2}, \\ v_{c4}(t) \rightarrow -M R_t T_c \omega \frac{[(T_c \omega + \omega \tau) \cos(\omega t) + (T_c \omega^2 \tau - 1) \sin(\omega t)]}{(1 + T_c^2 \omega^2)(1 + \tau^2 \omega^2)}. \end{cases} \quad (9)$$

As shown in Eq. (9), both  $v_{c2}$ ,  $v_{c3}$ , and  $v_{c4}$  converge to sinusoidal waveforms. To investigate the influence of frequency  $\omega$  on the battery dynamics, the amplitudes of  $v_{c2}$ ,  $v_{c3}$ , and  $v_{c4}$  at different frequencies are shown in Fig. 2 for  $T_c = 80\text{sec}$ . As shown in Fig. 2, when the current frequency is “high” (i.e.,  $>0.1\text{Hz}$ ), the battery voltage is dominated by the term that is associated with the ohmic resistance. When the current frequency is “medium” (e.g.,  $0.004\text{Hz}$ ), the SoC variation voltage can be neglected.

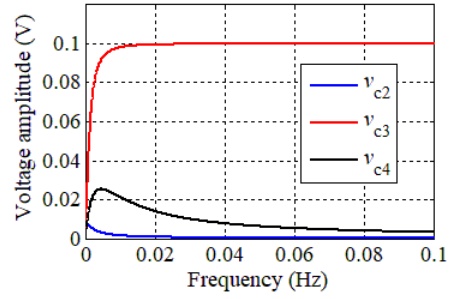


Fig. 2. Battery voltage components at various current frequencies.

The reason is that only the low-frequency current induces a significant SoC change. When the current frequency is “low” (e.g.,  $0.0004\text{Hz}$ ),  $v_{c2}$ ,  $v_{c3}$ , and  $v_{c4}$  should all be considered. Therefore, by incorporating a high-pass filter, the battery voltage components can be “stripped out” by injecting battery current waveforms of different frequencies. We point out that the analysis shown above should be conducted for different battery chemistries, where the frequency ranges may slightly change.

### III. CRAMER-RAO BOUND ANALYSIS

#### A. The time-averaged Cramer-Rao bound

The CR bound can be used to quantify estimation accuracy [13]. The process for computing the time-averaged CR bound is briefly introduced below. The sensitivity of the voltage measurement  $v_b$  to the  $i^{\text{th}}$  parameter  $\theta_i$  in the time domain can be expressed using the inverse Laplace transform  $\mathcal{L}^{-1}$ :

$$\frac{\partial v_b}{\partial \theta_i}(t) = \mathcal{L}^{-1} \left[ \frac{\partial v_b}{\partial \theta_i}(s) \right]. \quad (10)$$

Assuming Gaussian noise in the measurement of  $v_b$ , the time-averaged Fisher information matrix  $\bar{\mathbf{F}}_c$  can be calculated when the battery current  $i_b(t)$  is a periodic signal with period  $2\pi/\omega$ . The details of this calculation are provided in [11].

$$\bar{\mathbf{F}}_c = \frac{1}{\sigma_v^2} \frac{\omega}{2\pi} \begin{pmatrix} \int_0^{2\pi} \left( \frac{\partial v_b}{\partial \theta_1} \right)^2 dt & \int_0^{2\pi} \frac{\partial v_b}{\partial \theta_1} \frac{\partial v_b}{\partial \theta_2} dt & \dots & \int_0^{2\pi} \frac{\partial v_b}{\partial \theta_1} \frac{\partial v_b}{\partial \theta_N} dt \\ \vdots & \vdots & \ddots & \vdots \\ \int_0^{2\pi} \frac{\partial v_b}{\partial \theta_N} \frac{\partial v_b}{\partial \theta_1} dt & \int_0^{2\pi} \left( \frac{\partial v_b}{\partial \theta_2} \right)^2 dt & \dots & \int_0^{2\pi} \frac{\partial v_b}{\partial \theta_2} \frac{\partial v_b}{\partial \theta_N} dt \\ \vdots & \vdots & \ddots & \vdots \\ \int_0^{2\pi} \frac{\partial v_b}{\partial \theta_N} \frac{\partial v_b}{\partial \theta_1} dt & \int_0^{2\pi} \frac{\partial v_b}{\partial \theta_N} \frac{\partial v_b}{\partial \theta_2} dt & \dots & \int_0^{2\pi} \left( \frac{\partial v_b}{\partial \theta_N} \right)^2 dt \end{pmatrix}, \quad (11)$$

where  $\boldsymbol{\theta} = [\theta_1, \theta_2, \dots, \theta_N]$  is the vector of parameters to be identified and  $\sigma_v^2$  is the variance of the battery voltage measurement noise. The CR bounds can then be obtained by inverting the Fisher information matrix:

$$\text{cov}(\theta_i) \geq \underline{\sigma}^2(\theta_i) = \text{diag}(\bar{\mathbf{F}}_c^{-1})_i, \quad (12)$$

where the over bar symbol ( $\bar{\cdot}$ ) denotes a time-averaged value,  $\text{cov}(\theta_i)$  is the variance of the estimation error for  $\theta_i$ ,  $\underline{\sigma}^2(\theta_i)$  is the CR lower bound of  $\theta_i$ , indicating the

minimum achievable variance, and  $\text{diag}(\bar{\mathbf{F}}_c^{-1})_i$  is the  $i^{\text{th}}$  diagonal element of  $\bar{\mathbf{F}}_c^{-1}$ .

### B. Sequential algorithm

The sequential algorithm includes three steps, as illustrated below.

Step #1: The ohmic resistance is estimated by using a high-pass filter and injecting a high-frequency current.

Step #2: The estimated ohmic resistance is then used in the estimation of  $R_t$  and  $\tau$ , which are estimated by using a high-pass filter and injecting medium-frequency current.

Step #3: Based on the estimated  $R_s$ ,  $R_t$ , and  $\tau$ , the SoC and SoH are then simultaneously estimated.

The CR bounds of the filtered system are derived following the process shown in section 3.1. Based on Eq. (6) it can be seen that, by injecting high-frequency current, the filtered system can be simplified as

$$v_{\text{bf}}(s) \approx -R_s i_{\text{bf}}(s). \quad (13)$$

Therefore, the ohmic resistance  $R_s$  can be estimated solely in the first step. By using the sinusoidal current shown in Eq. (8), the asymptotic sensitivity and the time-averaged CR bound of  $R_s$  can be given as

$$\begin{aligned} \frac{\partial v_{\text{bf}}}{\partial R_s}(t) &= -MT_c\omega \frac{T_c\omega \cos(\omega t) - \sin(\omega t)}{T_c^2\omega^2 + 1}, \\ \underline{\sigma}(R_s) &= \frac{\sqrt{2}\sigma_v \sqrt{T_c^2\omega^2 + 1}}{MT_c\omega}. \end{aligned} \quad (14)$$

This shows that the estimation accuracy of  $R_s$  can be improved by decreasing the voltage measurement noise  $\sigma_v$  and the cut-off frequency (i.e.,  $1/T_c$ ) as well as increasing the current amplitude and frequency. Note that  $1/T_c$  cannot be too low, especially when the battery current involves medium-frequency components, as the dynamics of the RC pair should also be considered and it makes the simplification in Eq. (13) inaccurate, as shown in Fig. 2.

When the medium-frequency current is injected, the filtered system can be simplified as follows:

$$V_{\text{bf}}(s) = -\hat{R}_s i_{\text{bf}}(s) - \frac{R_t}{1 + \tau s} i_{\text{bf}}(s), \quad (15)$$

where  $\hat{R}_s$  is the estimated ohmic resistance that can be used in the second step to estimate  $R_t$  and  $\tau$ . The asymptotic sensitivities and time-averaged CR bounds of  $R_t$  and  $\tau$  can therefore be obtained as follows:

$$\begin{aligned} \frac{\partial v_{\text{bf}}}{\partial R_t}(t) &= -MT_c\omega \frac{T_c\omega \cos(\omega t) - \sin(\omega t) + \omega\tau \cos(\omega t)}{(T_c^2\omega^2 + 1)(\tau^2\omega^2 + 1)}, \\ \frac{\partial v_{\text{bf}}}{\partial \tau}(t) &= \frac{[(T_c\omega - T_c\omega^3\tau^2 + 2\omega\tau)\sin(\omega t) + (1 - \omega^2\tau^2 - 2T_c\omega^2\tau)\cos(\omega t)]}{(T_c^2\omega^2 + 1)(\tau^2\omega^2 + 1)^2 / (-MT_c\omega^2 R_t)}, \\ \underline{\sigma}(R_t) &= \frac{\sigma_v (\tau^2\omega^2 + 1) \sqrt{2(T_c^2\omega^2 + 1)}}{MT_c\omega}, \\ \underline{\sigma}(\tau) &= \frac{\sigma_v (\tau^2\omega^2 + 1)(T_c^2\omega^2 + 1) \sqrt{2(T_c^2\omega^2 + 1)}}{MT_c\omega^2 R_t}. \end{aligned} \quad (16)$$

It is clear that the estimation of the RC pair (i.e.,  $R_t$  and

$\tau$ ) can be improved by decreasing  $\sigma_v$  (i.e., measurement noise) and increasing  $M$  (i.e., signal amplitude). However, the influences of  $1/T_c$  and  $\omega$  are complex and will be numerically analyzed. Based on the above estimated parameters, the battery SoC and SoH can be estimated using Eq. (5). The asymptotic sensitivities and time-averaged CR bounds of  $z_0$  and  $1/Q_b$  are

$$\begin{aligned} \frac{\partial v_{\text{bf}}}{\partial z_0}(t) &= a, \quad \frac{\partial v_{\text{bf}}}{\partial (1/Q_b)}(t) = \frac{M\eta \sin(\omega t)}{\omega}, \\ \underline{\sigma}(z_0) &= \frac{\sigma_v}{a}, \quad \underline{\sigma}(1/Q_b) = \frac{\sqrt{2}\sigma_v \omega}{M\eta}. \end{aligned} \quad (17)$$

The estimation of SoC only depends on the OCV slope  $a$ . The estimation accuracy of  $1/Q_b$  can be improved by decreasing the current frequency as the battery capacity influences the battery terminal voltage via the SoC change, and therefore the detectable voltage variation requires a large SoC change. It is obvious and intuitive that the estimation accuracy can be increased by reducing noise and increasing current amplitude, as the SoC estimation accuracy can be improved when the battery has a more detectable voltage change. We point out that the quantified relationships presented in this paper can be used to evaluate the influences of different estimation techniques, which involve different amounts of uncertainty, on the estimation accuracy. Specifically, the improvement of the sequential algorithm is quantified when compared to the case where all parameters/states are estimated simultaneously, as will be shown in the sequel. The quantified relationships are important in the design of different estimation techniques and theoretically prove the effectiveness of the new design.

In this paper the CR bounds of estimated parameters/states under the sequential algorithm are compared with the multi-parameter case. According to the analysis in [17], two sinusoidal waveforms with the same amplitudes and with frequencies of  $\omega$  and  $5\omega$  are used in the multi-parameter case to persistently excite the battery. The same amplitudes are chosen to simplify the analysis, while the frequencies of  $\omega$  and  $5\omega$  were determined based on the CR bound analysis, which shows that the good performance is achieved when the frequency ratio is 5 [17].

Regarding the sequential algorithm, high-pass filters are adopted to ensure that the battery dynamics induced by the injected signals can be extracted for estimation purposes. The cut-off frequencies of the high-pass filters for estimating ohmic resistance and RC pair were set to 0.05Hz and 0.001Hz, respectively as the frequencies of the injected current were 0.5Hz and 0.02Hz. In the comparison the single-parameter case, which only estimates one parameter (or state) and assumes all other parameters/states to be well known, is considered as the benchmark. The CR bounds of SoC are not shown because they are same for all cases. The CR bounds are shown in Fig. 3, and some remarks can be given as below:

**Remark 1.** The single-parameter case has the best estimation performance over all conditions since the least uncertainty is involved.

**Remark 2.** For  $R_s$ , the estimation performance of the sequential algorithm is slightly worse than the multi-parameter case at low frequency due to the use of high-

pass filter. However, when the frequency increases, the estimation performance of the sequential algorithm is better due to the reduction of uncertainty. In addition, the sequential algorithm achieves much better performance when estimating the RC pair.

**Remark 3.** The SoC estimation accuracy of the sequential algorithm is the same as that of the single-parameter case, and much better than the multi-parameter case.

**Remark 4.** For the multi-parameter case there is a trade-off between  $R_s$  and RC pair. As a result, the optimal frequencies, which can achieve a good performance for all estimated parameters, are set to 0.002Hz and 0.01Hz.

#### IV. SIMULATION RESULTS

To verify the analysis in Section 3, simulations were conducted based on the first-order ECM, as shown in Fig. 4. The battery parameters listed in Table 1 were adopted. Note that the OCV-SoC curve of lithium-ion batteries generally presents nonlinear characteristics. The OCV-SoC curve for the studied battery cell is shown in Fig. 5, which indicates that the OCV-SoC curve can be approximately linearized over the SoC range of 50%-90% where the slope is approximately 8.8mV per 1% SoC variation. It means that when the battery SoC changes 1% the battery OCV changes 8.8mV averagely over the SoC range of 50%-90%. To simplify the Cramer-Rao bound analysis, a linearized OCV-SoC curve is used, while the nonlinear OCV-SoC curve is used in the simulation model as well as in the sequential algorithm. In addition, in the simulation white noise signals are generated in Matlab® and then added to the voltage measurement generated by the simulation model shown in Fig. 4.

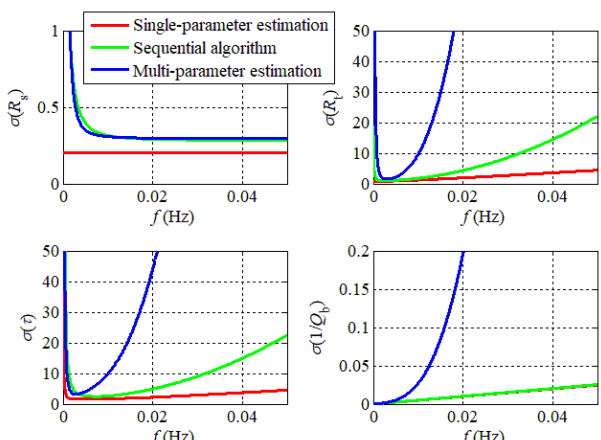


Fig. 3. The CR bounds results.

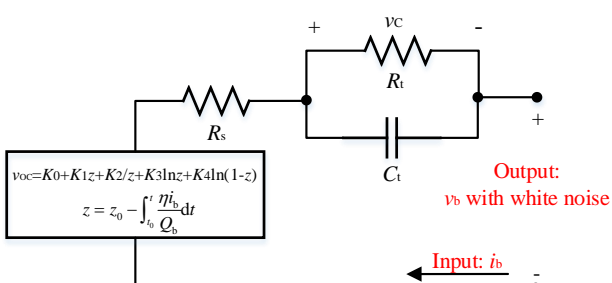


Fig. 4. Simulation model of the first-order circuit.

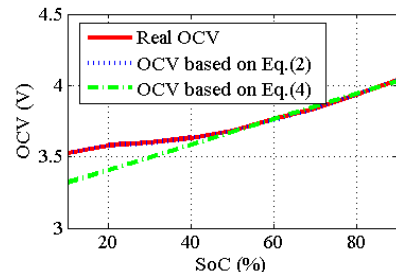
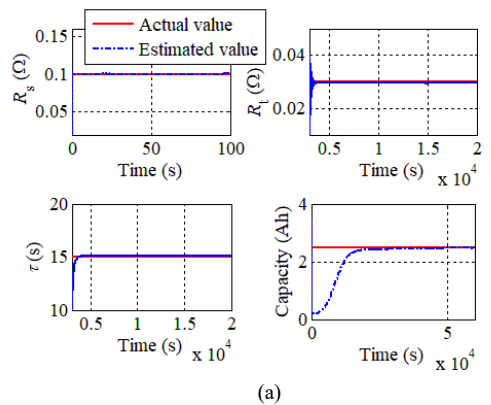


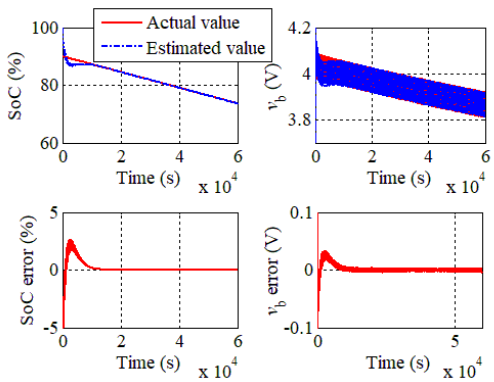
Fig. 5. OCV-SoC curve of the adopted Samsung ICR18650-26H cell.

In the multi-parameter case, the multi-scale extended Kalman filter (EKF), which has been proven to have good performance [3], is used to simultaneously estimate all parameters and states. The optimal current profile, which includes 3 sinusoidal waveforms with frequencies of 0.002Hz, 0.01Hz, and 0.005Hz, is used in the multi-parameter case. We point out that two frequencies are included in the CR bound analysis for the four estimated parameters, since the SoC estimation is independent of the current frequency. However, SoC is also estimated in the simulation, therefore the 0.005Hz waveform is an additional component to persistently excite the system because in total 5 parameters/states are estimated [7]. For the sequential algorithm, according to the CR bound results shown in Fig. 3, we incorporate a first-order high-pass filter (3dB bandwidth of 0.05Hz) and inject a 0.5Hz sinusoidal current with an amplitude of 0.5C (i.e., 1.22A) to estimate  $R_s$ . This value is then used in the second step to estimate  $R_t$  and  $\tau$  by injecting a 0.02Hz sinusoidal current with an amplitude of 0.5C. A first-order high-pass filter with 3dB bandwidth at 0.001Hz is adopted. The EKF is used in the above steps. After obtaining the above parameters, a combined SoC/SoH estimation is finally conducted using the dual EKF. Two sinusoidal currents (0.01Hz and 0.05Hz) and a DC current (all current amplitudes are 0.02 C rate) are used. For a fair comparison, the initial guesses of the estimated parameters/states are the same for both the multi-parameter and sequential algorithm cases, which are set to  $[R_s(0) \ R_t(0) \ \tau(0) \ 1/Q_b(0) \ SoC(0)]^T = [0.02 \ 0.01 \ 10 \ 1/2 \ 1]^T$ . White noise with the standard variance of 10mV is added to the battery voltage measurement. Note that the frequency of the injected current depends on the battery parameters. For example, for some battery types, the time constant of the RC pair is much smaller than the one of the studied battery cell. As a result, the frequencies of the injected current for ohmic resistance and RC pair estimation should be increased to strip out the battery dynamics dominated by the parameter in question. The frequency can be selected based on the battery dynamic analysis, as shown in Fig. 2. We point out that the selected frequencies for the injected current may not be able to be adopted to other types of batteries. But the same analysis presented in this paper can be followed for the frequency selection, which does not influence the effectiveness of the proposed algorithm.

The simulation results are shown in Fig. 6 and Fig. 7. Note that the actual states are generated using the simulation model shown in Fig. 4 together with the battery parameters given in Table 1.

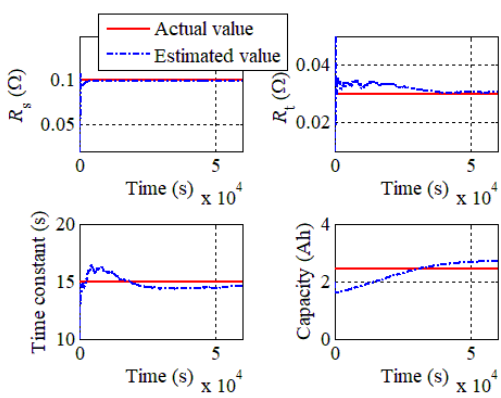


(a)

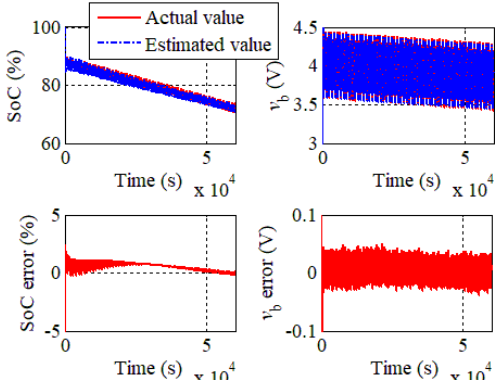


(b)

Fig. 6. Simulation results of the sequential algorithm. (a) Parameter estimation results. (b) State estimation results.



(a)



(b)

Fig. 7. Simulation results of the multi-parameter case. (a) Parameter estimation results. (b) State estimation results.

Regarding  $R_s$ , both cases have satisfactory estimation performance. In addition, although the best performance of the multi-parameter case is obtained using the optimal current profile, the sequential algorithm still achieves much better performance when estimating RC pair parameters, SoC, and SoH. The CR bound analysis shown in Section 3 is therefore verified. When the estimation of parameters and states can be separated and conducted sequentially, the estimation accuracy can be significantly improved since less uncertainty is involved.

## V. EXPERIMENTAL RESULTS

To verify the CR bound analysis and the effectiveness of the sequential algorithm, experiments were conducted using a Lithium ion battery cell, whose parameters can be found in Table 1. As shown in Fig. 8, the test bench consists of an ARBIN@ BT2000 tester, a temperature chamber, and the MITS pro system used for programming the current profile and monitoring the battery [26]. The battery cell is placed in the temperature chamber, which is accurately controlled to provide a constant temperature environment during the experiment. The voltage and current of the battery cell are measured by the ARBIN@ tester and then sent to a computer through TCP/IP communication. Unlike the simulation, the battery parameters are changing in the experiment as they depend on SoC, and errors caused by unmodeled dynamics are also introduced. The “actual values” of battery parameters were calculated based on the HPPC test. The experiment was conducted at 20°C and an initial battery SoC of 60%. The initial values of the estimated parameters are chosen to be  $[\hat{R}_s(0) \hat{R}_t(0) \hat{\tau}(0) \hat{Q}_b(0)] = [0.02 \ 0.03 \ 15 \ 2]$ , and the initial values of estimated SoC and  $v_c$  were set to 30% and 0V, respectively.

In Step #1, a 0.5Hz sinusoidal current with an amplitude of 0.5C was injected, as shown in Fig. 9(a). The first-order Butterworth high-pass filter used had a 3dB bandwidth of 0.05Hz. As shown in Fig. 9(b), the estimated  $R_s$  can accurately track the actual value. In Step #2, a 0.02Hz sinusoidal current with an amplitude of 0.5C was added to a “base” current (0.004Hz sinusoidal current with amplitude of 0.5C), as shown in Fig. 9(a).

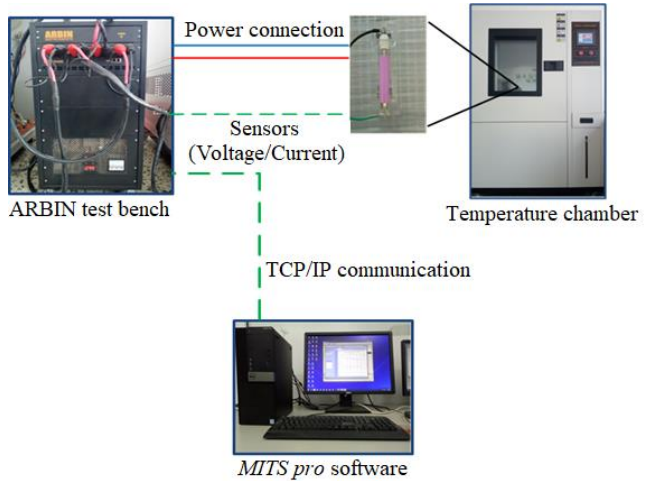


Fig. 8. Experimental test bench [26]

The first-order butterworth high-pass filter used had a 3dB bandwidth of 0.002Hz. By using the estimated  $R_s$ , the estimated  $R_t$  and  $\tau$  can largely track the real values, even though the estimated  $R_t$  has a static error when compared to its “actual value”, as shown in Fig. 9(c). This indicates that the first-order ECM model has limitations, since the RC pair is difficult to be characterized and estimated.

Finally, in step #3, the estimated  $R_s$ ,  $R_t$ , and  $\tau$  are used to estimate SoC and SoH concurrently. A scaled Bus Driving Cycle is used in Step #3 to represent a practical current profile for the battery. As shown in Fig. 9(d), the SoC estimation is accurate given that the estimated error is below 1.5% under a significant initial error (30%). As shown in Fig. 9(e), the estimated capacity  $Q_b$  converges to the actual value, which is obtained from the static capacity test, and there is no obvious error after convergence. Since all parameters/states are well estimated, the estimated terminal voltage also tracks the actual value well, as shown in Fig. 9(f).

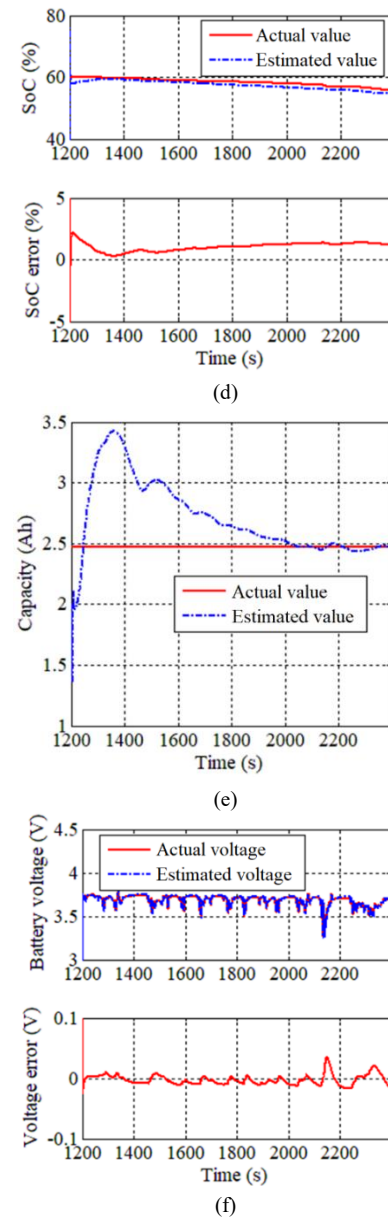
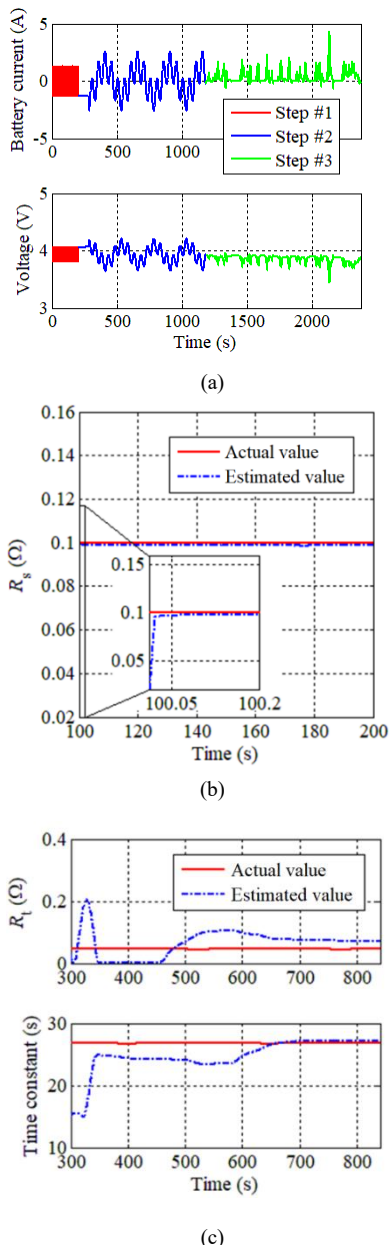


Fig. 9. Experimental results. (a) Battery current profile. (b)  $R_s$  estimation result (Step #1). (c)  $R_t$  and  $\tau$  estimation result (Step #2). (d) SoC estimation result (Step #3). (e)  $Q_b$  estimation result (Step #3). (f)  $v_b$  estimation result (Step #3).

Experimental results for the multi-parameter case have been shown in [17], [18] using the same Samsung 18650 battery cell. Due to space limitations, the experimental comparison is not provided in this paper. Based on the experimental results provided in [17], [18], it is clear that the sequential algorithm achieves much better estimation performance when compared to the multi-parameter case.

In terms of the implementation of the proposed method, we point out that, if the battery is the only power source, it is difficult to inject the high frequency current while keeping the system operating normally since the battery needs to satisfy the power demand. It may be feasible to manipulate the battery charging profile to inject the desired current signals for the parameter/state estimation, however, it is still difficult to implement the proposed algorithm as the charging process is not easy to be changed in most battery-only applications (e.g., the charging station for electric vehicles). Especially, when

the battery parameters under charging conditions significantly differ from the ones under discharging conditions, it is difficult to use the proposed sequential algorithm as the parameters, which are estimated in charging processes, cannot be used in discharging processes.

Furthermore, when the battery is adopted in over-actuated systems (e.g. the battery/supercapacitor hybrid energy storage system and hybrid electric vehicles), which have the additional power source and only follow one power demand, the desired current signals and output regulation objectives can be achieved concurrently, and estimation over a long period may not interrupt the normal operation. The optimal current for parameter identification of battery can be compensated by the other power source (e.g., supercapacitor). In addition, since the sinusoidal current is injected in the battery current profile, the corresponding compensation current for the other power source would not continuously drain its energy, meaning that it can be produced indefinitely. Specifically, given that the battery voltage is generally stable, the sinusoidal signal injected in battery will induce a corresponding sinusoidal power demand to the supercapacitor, meaning that the supercapacitor is not required to constantly discharge (or charge). For example, when there is no power demand from the load, the supercapacitor only needs to provide a periodic current with an average value of zero to compensate the injected signal. Therefore, only a small amount of energy is consumed due to losses in the power electronic components. In addition, without disturbing the current injection, the battery can be used to charge the supercapacitor in practical applications.

We note that the estimation process of the RC parameters takes a long time since  $R_t$  does not entirely converge to its actual value at 800s, as shown in Fig. 9 (c), and this may pose some problems in practical applications. We would like to point out that the RC voltage is small for the studied battery cell therefore the estimation of RC parameters is inherently difficult, but this in turn gives us some hints that the RC parameters can be potentially neglected for this specific battery cell when focusing on the SoC/SoH estimation from the battery modeling perspective, since the RC voltage only slightly contributes to the battery terminal voltage and hence would not significantly influence the SoC/SoH estimation accuracy. In future work, the trade-off between the model complexity and the estimation accuracy of battery states (e.g., SoC and SoH) will be further investigated.

## VI. CONCLUSION

The estimation of battery parameters and states based on a first-order ECM is studied in this paper. The CR bound is used to evaluate the parameter/state estimation accuracy for three cases: the single-parameter case, the multi-parameter case, and the sequential algorithm case. The analysis shows the possibility of improving estimation accuracy by injecting persistently exciting signals into the current waveform and estimating the parameters/states sequentially. The CR bound analysis shows that the estimation accuracy of sequential estimation is much better than that of the multi-parameter

case. The effectiveness of sequential estimation is verified by simulation results. The initial experimental result is also provided to further validate the proposed algorithm.

We note that the proposed algorithm is designed for over-actuated systems, since the over-actuation feature can be exploited for the active current injection. For the battery-only applications (e.g., electric vehicles), the feasibility of the proposed method should be further evaluated and it has limitations because generally the battery current profile cannot be changed for the signal injection.

## REFERENCES

- [1] Lu, X. Han, J. Li, J. Hua, and M. Ouyang, "A review on the key issues for lithium-ion battery management in electric vehicles," *J. power sources*, vol. 226, pp. 272-288, Mar. 2013.
- [2] J. Zhang and J. Lee, "A review on prognostics and health monitoring of Li-ion battery," *J. Power Sources*, vol. 196, pp. 6007-6014, Aug. 2011.
- [3] R. Xiong, F. Sun, Z. Chen, and H. He, "A data-driven multi-scale extended Kalman filtering based parameter and state estimation approach of lithium-ion polymer battery in electric vehicles," *Appl. Energy*, vol. 113, pp. 463-476, Jan. 2014.
- [4] X. Hu, S. Li, S and H. Peng, "A comparative study of equivalent circuit models for Li-ion batteries," *J. Power Sources*, vol. 198, pp. 359-367, Jan. 2012.
- [5] M. Charkhgard and M. Farrokhi, "State-of-charge estimation for lithium-ion batteries using neural networks and EKF," *IEEE Trans. Ind. Electron.*, , vol. 57, no. 12, pp. 4178-4187, Dec. 2010.
- [6] X. Lin and A. Stefanopoulou, "Analytic bound on accuracy of battery state and parameter estimation," *J. Electrochem. Soc.*, vol. 162, no. 9, pp. A1879-A1891, 2015.
- [7] P. Ioannou and J. Sun, *Robust adaptive control* (Vol. 1). North Chelmsford, MA, USA: Courier Corporation, 2012.
- [8] X. Lin, "A Data Selection Strategy for Real-time Estimation of Battery Parameters," in *American Control Conference (ACC)*, 2018, pp. 2276-2281.
- [9] Z. Song J. Hou, H. Hofmann, X. Lin, and J. Sun, "Parameter Identification and Maximum Power Estimation of Battery/Supercapacitor Hybrid Energy Storage System based on Cramer-Rao Bound Analysis," *IEEE Trans. Power Electron.*, 2018.
- [10] P. Mishra, M. Garg, S. Mendoza, J. Liu, C. Rahn, H. Fathy, "How does model reduction affect lithium-ion battery state of charge estimation errors? Theory and experiments," *J. Electrochem. Soc.*, vol. 164, no. 2, pp. A237-A251, 2017.
- [11] X. Lin, "Analytic Analysis of the Data-Dependent Estimation Accuracy of Battery Equivalent Circuit Dynamics," *IEEE Contr. Syst. Letters*, vol. 1, no. 2, pp. 304-309, Jun. 2017.
- [12] A. Klintberg, T. Wik, and B. Fridholm, "Theoretical bounds on the accuracy of state and parameter estimation for batteries," in *American Control Conference (ACC)*, 2017, pp. 4035-4041.
- [13] M. Rothenberger, D. Docimo, M. Ghanaatpishe, and H. Fathy, "Genetic optimization and experimental validation of a test cycle that maximizes parameter identifiability for a Li-ion equivalent-circuit battery model," *J. Energy Storage*, vol. 4, pp. 156-166, Dec. 2015.
- [14] M. Rothenberger, J. Anstrom, S. Brennan, H. Fathy, "Maximizing parameter identifiability of an equivalent-circuit battery model using optimal periodic input shaping," in *ASME 2014 Dynamic Systems and Control Conference*, 2014, pp. V001T19A004-V001T19A004.
- [15] X. Lin, "Theoretical Analysis of Battery SOC Estimation Errors under Sensor Bias and Variance," *IEEE Trans. Ind. Electron.*, vol. 65, no. 9, pp. 7138-7148, Sep. 2018.
- [16] Y. Zheng, M. Ouyang, X. Han, L. Lu, J. Li, "Investigating the error sources of the online state of charge estimation methods for lithium-ion batteries in electric vehicles," *J. Power Sources*, vol. 377, pp. 161-188, Feb. 2018.
- [17] Z. Song, X. Wu, X. Li, J. Sun, H. Hofmann, H. Jun, "Current profile optimization for combined state of charge and state of health estimation of Lithium ion battery based on Cramer-Rao bound analysis," *IEEE Trans. POWER ELECTR.*, 2018.
- [18] Z. Song, J. Hou, X. Li, X. Wu, X. Hu, H. Hofmann, J. Sun, "The sequential algorithm for combined state of charge and state of health estimation of Lithium ion Battery based on active current injection," *arXiv*

*preprint arXiv:1901.06000.*

- [19] J. Xu, C. Mi, B. Cao, J. Cao, "A new method to estimate the state of charge of lithium-ion batteries based on the battery impedance model," *J. Power Sources*, vol. 233, 277-284, Jul. 2013.
- [20] D. Di Domenico, A. Stefanopoulou, G. Fiengo, "Lithium-ion battery state of charge and critical surface charge estimation using an electrochemical model-based extended Kalman filter," *J. Dyn. Syst. Meas. Control*, vol. 132, no. 6, 061302, Oct. 2010.
- [21] C. Weng, Y. Cui, J. Sun, and H. Peng, "On-board state of health monitoring of lithium-ion batteries using incremental capacity analysis with support vector regression," *J. Power Sources*, vol. 235, pp. 36-44, Aug. 2013.
- [22] J. Wei, G. Dong, and Z. Chen, "Remaining Useful Life Prediction and State of Health Diagnosis for Lithium-Ion Batteries Using Particle Filter and Support Vector Regression," *IEEE Trans. Ind. Electron.*, vol. 65, no. 7, pp. 5634-5643, Jul. 2018.
- [23] X. Lin, H. Perez, S. Mohan, J. Siegel, A. Stefanopoulou, Y. Ding, and M. Castanier, "A lumped-parameter electro-thermal model for cylindrical batteries," *J. Power Sources*, vol. 257, pp. 1-11, Jul. 2014.
- [24] N. Samad, J. Siegel, and A. Stefanopoulou, "Parameterization and validation of a distributed coupled electro-thermal model for prismatic cells," in *ASME 2014 Dynamic Systems and Control Conference*, 2014, pp. V002T23A006-V002T23A006.
- [25] H. He, R. Xiong, X. Zhang, F. Sun, and J. Fan, "State-of-charge estimation of the lithium-ion battery using an adaptive extended Kalman filter based on an improved Thevenin model," *IEEE Trans. Veh. Technol.*, vol. 60, no. 4, pp. 1461-1469, Mar. 2011.
- [26] X. Wu, X. Li, and J. Du, "State of Charge Estimation of Lithium-Ion Batteries Over Wide Temperature Range Using Unscented Kalman Filter," *IEEE Access*, vol. 6, pp. 41993-42003, Aug. 2018.